An Electron Diffraction Study of Mannan I. Crystal and Molecular Structure

Henri Chanzy* and Serge Pérez[†]

Centre de Recherches sur les Macromolécules Végétales,[‡] *CNRS, Grenoble, BP 68, 38402 Saint Martin d'Hères Cedex, France*

Donald P. Miller

Department of Physics and Astronomy, Clemson University, Clemson, South Carolina 29631

Gaio Paradossi

Dipartimento di Chimica, Universita di Napoli, 80134 Napoli, Italy

William T. Winter*

Department of Chemistry and Polymer Research Institute, Polytechnic University, Brooklyn, New York 11201. *Received December 8, 1986*

ABSTRACT: The crystal and molecular structure of Mannan I has been determined by a constrained linked-atom least-squares refinement utilizing intensities derived from electron diffraction and stereochemical restraints. In this polymorph, chains crystallize on an orthorhombic lattice with a = 0.892 nm, b = 0.721 nm, and c = 1.027 nm. Systematic absences are consistent with the space group $P2_12_12_1$. A density of 1.57 g·cm^{-3} requires four mannose residues per unit cell, indicating that the chemical repeating unit is also the crystallographic asymmetric unit. Intensities were measured from diffraction patterns produced by specimens which were arranged with c^* either parallel to the electron beam or rotated about a^* or b^*. Several zones including [001], [0$\bar{1}$1], and [$\bar{1}$01] were collected, digitized, and reduced to integrated intensities. The best model obtained using the base plane data coupled with a stereochemical refinement model yields R = 0.245 and R'' = 0.221. It corresponds to a system of highly extended 2-fold helices stabilized by intramolecular O3···O5 hydrogen bonds and packing into (110) sheets of alternately "up" and "down" chains along the apparent growth plane. The association of adjacent chains is stabilized by intermolecular O2···O5 hydrogen bonds. The (Φ,Ψ) angle pair defining the main chain conformation is (−81.1°, −160.8°), and O6 is arranged in an approximately *gt* fashion. Subsequently attempts were made to incorporate the intensities from higher layer lines into the refinement process.

Introduction

The native crystal and molecular structure of poly-[(1→4)β-D-mannose] or mannan is of interest for at least three separate reasons. First, there is the structural similarity with cellulose which offers an opportunity to investigate the effects of configurational alterations in substituent placement and the concomitant charge distribution changes. Secondly, Nieduszynski and Marchessault[1] have used a limited set of X-ray intensities coupled with a hard-sphere potential energy approach to compare different models of the mannan secondary structure and crystal packing. Their studies favored a model in which nearest-neighbor chains pass through the crystal lattice in opposite directions, i.e. antiparallel chains. Conversely, X-ray diffraction[2,3] and electron microscopy[4] studies of cellulose suggest that its native form involves crystallization through the association of parallel chains into a crystal structure. A definitive assignment of chain sense in these crystalline domains is essential to any consideration of the in vivo mechanisms leading to their formation.

Finally, there are appreciable similarities between the lattice constants of mannan[5] and the more complex galactomannan gums[6–8] such as guar, tara, and locust bean or carob. This observation suggests the conservation of packing features observed in mannan into the galactomannan family.

Mannan can be obtained as a pure homopolymer from the endosperm of certain plants, notably ivory nut, *Phytelephas macrocarpa*,[9] as well as from the walls of alga belonging to the families *Codiaceae* and *Dasycladaceae*.[10] Both the plant and algal materials exhibit in situ crystallinity although only the latter are optically anisotropic in the light microscope. The algal mannans have been reported to exist in two different polymorphs, the first similar to that observed with ivory nut mannan being referred to as mannan I and the second, in analogy with cellulose polymorphism, as mannan II. The second structure is thought to be a hydrate. Similar molecules, called glucomannans, where β-D-glucosyl residues replace some of the mannosyl units in an apparently aperiodic fashion can be obtained from the cell walls of coniferous trees and the seed endosperm of various plants, such as *Tubera salep* and *Amorphophallus konjac*. Following an initial demonstration by Bittiger and Husemann[11] that mannan could be induced to form polymer single crystals by precipitation from solvents such as aqueous butanol, workers in this laboratory have prepared mannan I type crystals from mannans and glucomannans of various origins.[12,13] Independent of the glucose/mannose ratio, the lattice constants remained relatively invariant suggesting that the association of mannan chains in mannan I could accommodate irregular main-chain insertions of glucose moieties in an essentially isomorphous fashion.

Attempts at determining a detailed structure model for mannan began with the work of Frei and Preston[5] although Meyer and Mark[14] recognized structural similarities with cellulose from the diffraction patterns of the two compounds. Analysis of the X-ray data obtained from mannans has been complicated by the presence of additional phases and other impurities in the specimens. As a consequence, the intensities of individual maxima have been determined by visual estimates of the additional intensity

[†] Present address: Laboratorie de Physicochimie, Macromoléculaire, INRA, Chemin de la Géraudière, Nantes, F-44072 France.

[‡] Affiliated with the Université Scientifique Technologique et Médicale de Grenoble, France.

0024-9297/87/2220-2407$01.50/0

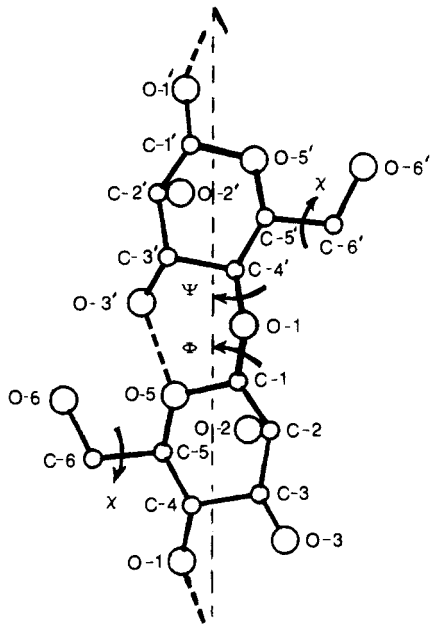

Figure 1. The atomic labeling scheme for the mannan chain and designation of the conformation angles Φ, Ψ, and χ.

above background levels. The resulting data have been characterized by the apparent absences of several reflections predicted from the lattice constants and not expected to be systematically absent.[1]

Verification that these reflections are, in fact, weak and the generation of models which correctly predict the intensity distribution is an essential component of the structure modeling process, and for this reason we have attempted to use the electron diffraction intensity data obtained from the mannan I single crystals, thereby experimentally separating the scattering contribution of this single phase from that due to the various contaminants. Using the *hk*0 intensities coupled with a nonbonded potential energy term arbitrates between the competing crystal[1] and conformation[15,16] models which have been proposed for mannan. Finally, since other reflection zones including [0,−1,1] and [−1,0,1], corresponding to reflection classes *hkk* and *hkh*, can be examined by rotation of the lamellar single crystals about a^*b^*, we sought to explore the problems which might be encountered with incorporation of electron diffraction intensity data obtained from tilted crystals.

Materials and Methods

Nomenclature. The relative orientation of two contiguous (1 → 4) linked β-D-mannose residues is given by torsional angles Φ and Ψ, which are defined by the four-atom sequences O5–C1–O1–C4′ and C1–O1–C4′–C5′, respectively. Other conformational parameters are the orientations of the primary hydroxyl groups around C5–C6 bonds. The conformation is referred to as either gauche-trans, gauche-gauche, or trans-gauche. In this terminology, the torsion angle θ(O5–C5–C6–O6) is stated first, followed by the torsion angle θ(C4–C5–C6–O6).[17] The sign of the torsion angles is defined in agreement with the rules recommended by the IUPAC-IUB Commission of Biochemical Nomenclature. These parameters, together with the atom labeling scheme, are shown in Figure 1.

Experimental Details. Ivory nut mannan, a gift of T. E. Timell,[18] was used in this work. The "A" fraction, as defined by Lüdtke,[19] was prepared and triacetylated following the procedure for unfractionated mannans previously described by us.[12] The acetylated product was dissolved in chloroform and fractionated on a Styragel column. The fraction collected at 200–300 cm³ was used for subsequent crystallization experiments. Analytical HPLC of this fraction indicated a DP_n of 13 for this mannantriacetate (MTA). In the final crystallization process 7 mg of MTA was dissolved in 5% (w/v) NaOH (5 cm³), stirred for 3 h at room temperature, and dialyzed for 12 h against distilled water yielding a slightly turbid mannan solution.

A crystallization bomb[20] was set up with DMSO (1 cm³) inside the sealed glass ampule and the mannan solution (1 cm³) outside. The sealed bomb was heated to 120 °C, the DMSO ampule was broken, and its contents were allowed to mix with the mannan solution inside the bomb, yielding a slurry of finely divided mannan crystals in the DMSO/water mixture. These crystals were then washed by successive centrifugations from water/DMSO mixtures and finally suspended in methanol.

For electron diffraction studies, droplets of the resultant crystal suspension were allowed to dry on carbon-coated grids. Electron diffraction patterns were recorded on Ilfoset FT35 film using a Philips EM 400T electron microscope equipped with a rotating sample holder and operated at 120 kV. The crystals were similar in appearance to those reported in ref 12. The *hk*0 reflections were collected from crystals aligned perpendicular to the electron beam while (*h*,*k*,2*k*), (*h*,*k*,*k*), (*h*,2*k*,*k*), and (*h*,3*k*,*k*) reflection classes were collected by rotation of the crystal about a^* by ±54°, ±35°, ±19°, and ±13° corresponding to the [0,2,−1], [0,−1,1], [0,−1,2], and [0,−1,3] zones, respectively. Similarly, rotation of the crystal about b^* by ±41°, ±23°, and ±16° permitted collection of the *h*,*k*,*h*, 2*h*,*k*,*h*, and 3*h*,*k*,*h* reflection classes ([−1,0,1], [−1,0,2], and [−1,0,3] zones, respectively).

Diffraction patterns for various exposure times and rotations were digitized with a computer-controlled scanning microphotometer using 50-μm and a 20-μm aperture. The microphotometer was calibrated after each 10201 measurements by passing a stepped precision gray-scale filter through the transmitted beam while simultaneously observing a selected clear film region. Measured transmissivities were converted, by a polynomial fit of the gray scale, to optical densities. A 202 × 202 data array, covering the observable diffraction pattern, was collected.

Integrated intensities were obtained from the digitized data following procedures described elsewhere.[21,22] The four symmetry-related quadrants, each a 101 × 101 array, were heuristicly (measurement values >2 × mean deviation discarded) averaged. Beam spallation and background scatter effects were removed by the subtraction of radial polynomial functions, fitted to selected measurement values chosen midway between diffraction maxima. For each spot, observable above noise, the lowest closed optical density contour above noise level was determined and the intensity numerically integrated. The mean deviation of the surrounding noise was used to estimate the associated error for each spot.

The *hk*0 data set included 29 measurable, independent intensities, 6 systematic absences of the odd orders for *h*00 or 0*k*0, and 5 other reflections which were also below the observational threshold. The [0,−1,1] zone contained 10 observed reflections, 3 systematic absences, and 8 below threshold absences of the class *hkk* while the [−1,0,1] had 15 observed reflections, 2 systematic absences, and 6 below threshold reflections of the type *hkh*. Atomic form factors describing the scattering of electrons by C, O, and H were taken from ref 23.

Refinement of the structure involved minimization of a quantity, Ω, by the linked-atom least-squares procedure (LALS).[24,25] This quantity is defined by the relation

$$\Omega = \sum w_m(|{}_oF_m|^2 - k^2|{}_cF_m|^2) + \sum \epsilon_{ij} + \sum \lambda_q G_q \qquad (1)$$

Here, the first term seeks to optimize the agreement between the observed structure amplitudes, ${}_oF_m$, and those calculated from the model, ${}_cF_m$, where k is a scaling factor, which places the observed amplitudes on the same scale as the calculated values, w_m is a weight, and the summation is carried out over the m independent reflections. For weak maxima whose intensities were below the observational threshold, a value equal to one-third the minimum measurable intensity within the zone was assumed. For such "unobserved reflections" the contribution to the least-squares normal equations is defined to be 0 if ${}_cF_m < {}_oF_m$. For all reflections the value of ${}_oF_m$ was calculated as the square root of the measured intensity.

The second term in eq 1 provides a simple quadratic approximation to the nonbonded repulsion and is applied to all pairwise interactions between atoms i and j when the distance between them is less than some "standard" value. The "standard distance"

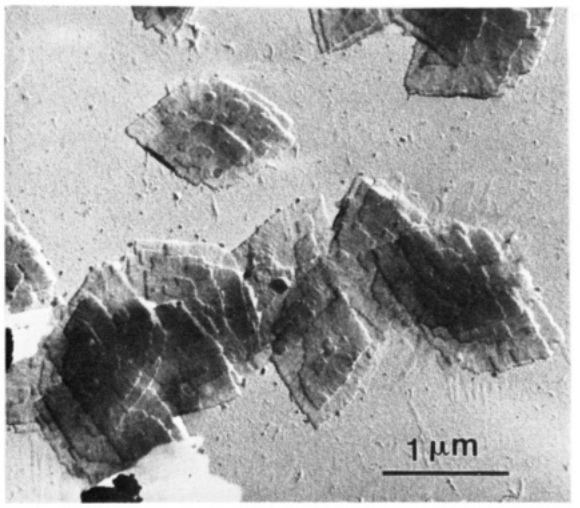

Figure 2. Transmission electron micrograph of a preparation of ivory nut mannan I crystals. The sample was shadowed with a W/Ta alloy.

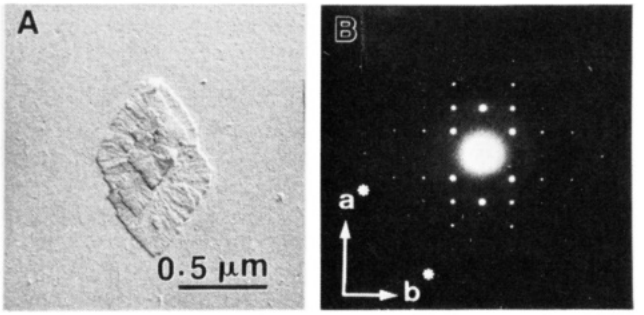

Figure 3. (A) Mannan I single crystal and (B) its associated $hk0$ electron diffraction pattern, properly oriented with respect to A.

and the coefficients used in this term are those previously employed by us.[26] The final term includes a set of coordinate constraint equations, G_q, together with their initially undefined Lagrangian multipliers, λ_q, and are used to preserve helix pitch and symmetry as well as, in the case of a flexible ring, ring closure.

Results

Diffraction Patterns and Crystallography. Figure 2 is a transmission electron micrograph showing the size and form of typical mannan I crystals used in this study. Figure 3 shows an isolated single crystal and the base plane electron diffraction pattern obtained from the untilted crystal. The a and b dimensions of the unit cell were derived from these patterns. Using previously reported values for the fiber repeat,[11] it was possible to calculate the appropriate tilt angles about a^* or b^* as shown in Figure 4. Figures 5 and 6 show the electron diffraction patterns obtained for various rotations of the crystals about a^* and b^*, respectively. Unit-cell parameters derived from the electron diffraction pattern of the present study were insignificantly different from our previously reported values of $a = 0.892$ nm, $b = 0.721$ nm, and $c = 1.027$ nm with all interfacial angles equal to 90°. We have interchanged the values of a and b to facilitate comparison with related structural studies.[7,8,15] Each pattern shown in Figures 5 and 6 has orthogonal symmetry. Furthermore, since identical diagrams with equal intensities are obtained when the crystals are rotated by $\pm\theta$ about either a^* or b^*, it can be concluded that the crystal structure of mannan I is truly orthorhombic. A map of the digitized intensity data derived from an untilted crystal after symmetry averaging and background filtering is shown in Figure 7. Data used in this study was recorded at approximately 50% of the crystallinity lifetime.

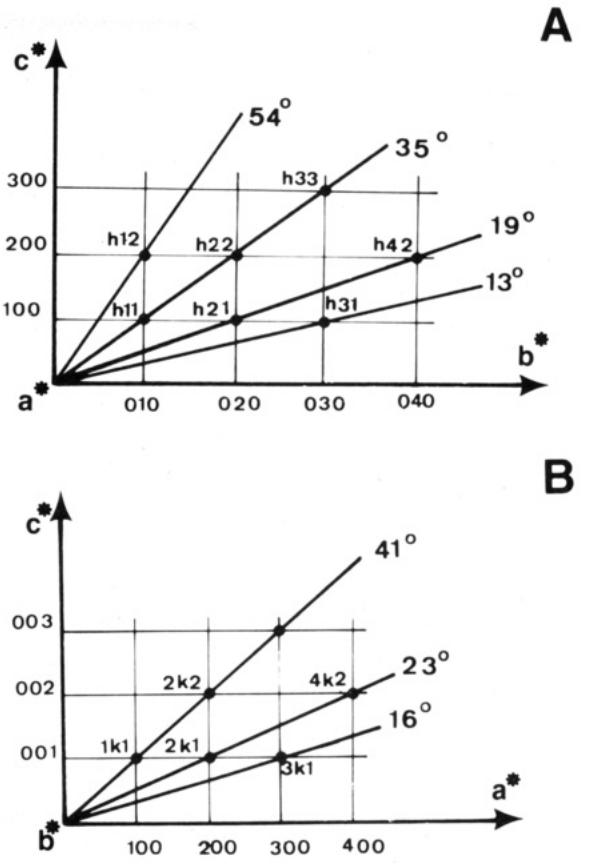

Figure 4. Schematic diagram showing the relationship between tilt angles and diffraction zones: A, tilt around a^*; B, tilt around b^*.

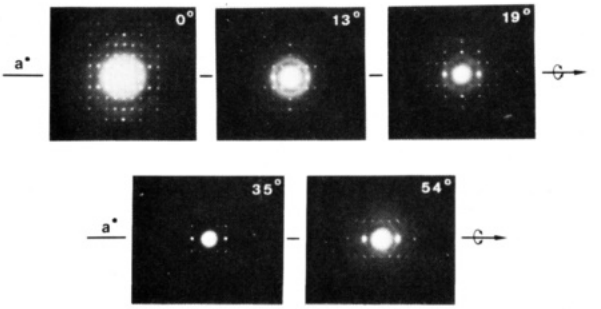

Figure 5. Electron diffraction patterns obtained from mannan I crystals rotated by ±13°, ±19°, ±35°, and ±54° around a^*, in comparison with an untilted diagram (tilt 0°). For each setting the same crystal was used for the positive and negative orientations and the resulting diagrams were identical in each case. Different crystals were used for each setting.

Examination of a considerable number of patterns from different zones and/or different crystals convinces us that the only verifiable systematic absences are those for classes (odd,0,0) and (0,odd,0). This determination is complicated by the considerable intensity of the 031 reflection which can, for thin, bent crystals, encroach upon the predicted position of the 030 reflection. Careful measurement of the centroid for this intensity establishes that its position is significantly greater than that expected for the 030. The electron diffraction data does not establish definitively the presence or absence of a corresponding systematic absence for the (0,0,odd) reflections. Coupled with the density,[10]

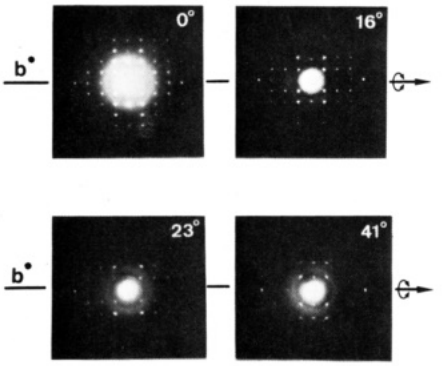

Figure 6. As in Figure 5 but the crystals were rotated about the b^* axis by ±16°, ±23°, and ±41°.

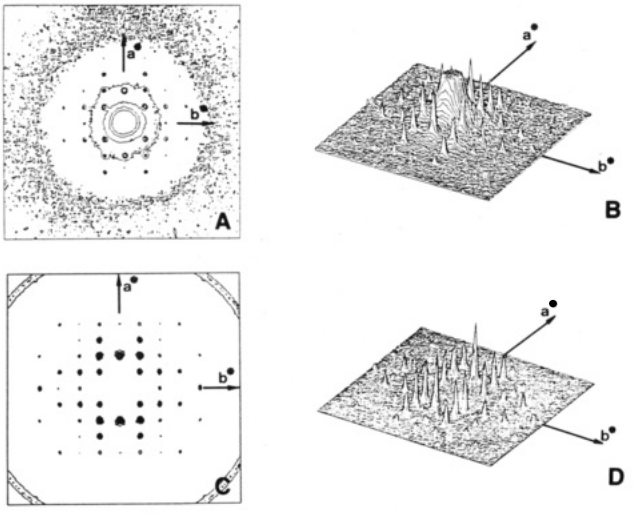

Figure 7. (A) Contoured projection of a digitized $hk0$ diffraction pattern of mannan I before background and noise removal. (B) As in A but in three-dimensional projection. (C) As in A but after background removal, symmetry averaging and noise reduction. (D) As in C but in three-dimensional projection.

structural formula for the repeating unit, and chirality of the molecule, it does establish that the space group must be either $P2_12_12_1$ or $P2_12_12$ and that the molecular chains pass through the unit cell in opposite directions.

Although the systematic absences, of themselves, provide sufficient reason for excluding a parallel chain mannan I model, we chose to include this possibility in the early stages of modeling. A conformational model of mannan I with twofold screw symmetry, a pitch of 1.027 nm, and minimal nonbonded interactions within the isolated chain was generated by minimizing the sum of the last two terms in eq 1. The resulting model had an O3′···O5 distance suggestive of an intramolecular hydrogen bond across each 1→4 linkage as is widely observed in other diequatorial β(1→4) linked glycans, e.g., cellulose or xylan but not pectin. This model chain was then placed in the unit cell with its helix axis parallel to c and coincident with a crystallographic 2_1 axis in the $P2_12_12_1$ space group. For the two antiparallel space groups, the second chain was generated by symmetry while for the parallel chain model the second chain was simply placed with its helix axis at $(a/2, b/2)$ relative to the first chain. The orientation of these two chains with respect to the unit cell edges a and b was then varied systematically in 10° increments and the crystallographic residuals[27] R and R'' for the $hk0$ data were computed at each point. In the parallel chain model this required a two-dimensional grid since the rotations of the two chains are independent. For the antiparallel model both space groups have the same projection down the c axis and so only a single calculation was required. The curves had two local minima at orientation angles, μ_1, of 58–60° ($R = R'' = 0.20$) and 100–105° ($R = 0.27$, $R'' = 0.25$). These two positions closely correspond with the "AP2" and "AP1" positions reported by Nieduszynski and Marchessault.[1] With the parallel chain model the lowest obtainable values in the R factor grid were $R = 0.32$ and $R'' = 0.44$ despite the additional degree of freedom inherent in this model. At this point the weight of the symmetry evidence implicit in the electron diffraction patterns coupled with the significantly poorer structure amplitude agreement caused us to reject any further consideration of parallel chain models for mannan I. Continued refinement of the structure led to a single model exhibiting $P2_12_12_1$ symmetry. The coordinates of atoms in the crystallographic repeat of this model are shown in Table I, a comparison of the observed and calculated structure amplitudes in Table II, and a summary of the values of varied parameters in Table III. The crystallographic residuals R and R'' for this model were 0.245 and 0.221, respectively.

Table I
Cartesian Coordinates (nm × 10^4) of Mannan I[a]

atom	x	y	z
C(1)	2250	543	3054
C(2)	3083	1248	1991
C(3)	2482	1029	611
C(4)	2284	−459	351
C(5)	1503	−1093	1497
C(6)	1371	−2595	1354
O(1)	2906	659	4273
O(2)	4411	739	2020
O(3)	3349	1580	−382
O(4)	1554	−659	−862
O(5)	2170	−850	2745
O(6)	1317	−3244	2623
H(1)	1330	935	3072
H(2)	3136	2224	2202
H(3)	1601	1498	552
H(4)	3175	−905	268
H(5)	582	−704	1530
H(6a)	2158	−2952	851
H(6b)	531	−2810	855

[a] (i) The helix axis for this residue is at $(a/4, 0, z)$. (ii) The second residue of this chain can be generated from the transform $(x', y', z') = (-x + a/2, -y, z + c/2)$. (iii) The second chain can be generated from the first chain by the transform $(x', y', z') = (x + a/2, y + b/2, -z)$.

Intensities from Higher Layers. With use of the model derived by refinement against the base plane data, structure amplitudes derived from the 35° and 41° tilted specimens were scaled to the $(hk0)$ data by varying only the electron diffraction scale factor k. For the (hkk) data obtained at 35° the values of R and R' were 0.367 and 0.314, respectively. For the (hkh) data obtained from the 41° diffraction pattern the values of R and R' were 0.368 and 0.352, respectively.

Discussion

The use of electron diffraction intensity data in the determination of crystal and molecular structure remains an area of some contention. What is clear from the present analysis and previous studies is that careful analysis of electron diffraction data derived from polymer single crystals does permit an unambiguous determination of lattice constants and symmetry elements in the base plane. Lattice constants derived from X-ray data suffer from ambiguities consequential to the projection of the entire $hk0$ plane onto a single line and concomitant problems in indexing. The question of symmetry elements such as 2_1

Table II
Final Values of the Observed, $_oF_{hkl}$, and Calculated, $_cF_{hkl}$, Structure Amplitudes[a]

h	k	l	$_oF_{hkl}$	$_cF_{hkl}$	h	k	l	$_oF_{hkl}$	$_cF_{hkl}$
0	1	0	sa	0.00	3	3	0	2.32	0.89
0	2	0	(6.89)	2.87	3	4	0	4.08	5.58
0	3	0	sa	0.00	3	5	0	7.00	4.39
0	4	0	15.97	17.99	4	0	0	6.92	0.99
0	5	0	sa	0.00	4	1	0	12.03	10.46
1	0	0	sa	0.00	4	2	0	6.92	8.91
1	1	0	27.22	30.76	4	3	0	9.56	4.80
1	2	0	13.29	8.82	4	4	0	5.24	4.75
1	3	0	14.17	14.36	4	5	0	6.18	2.16
1	4	0	(5.76)	1.98	5	0	0	sa	0.00
1	5	0	2.78	3.62	5	1	0	4.74	7.66
2	0	0	36.25	40.35	5	2	0	4.48	7.11
2	1	0	27.56	29.19	5	3	0	2.64	3.22
2	2	0	9.09	4.24	5	4	0	(1.00)	1.73
2	3	0	6.12	6.66	5	5	0	3.88	2.82
2	4	0	8.90	6.74	6	0	0	(1.00)	5.25
2	5	0	1.08	1.09	6	1	0	1.65	1.48
3	0	0	sa	0.00	6	2	0	2.71	2.09
3	1	0	20.13	17.18	6	3	0	(1.00)	2.79
3	2	0	6.18	1.78	6	4	0	2.24	1.41
			(b) Data Derived from the Crystal Tilted at 35°						
0	1	1	.88	0.95	3	1	1	4.45	0.99
0	2	2	3.46	6.26	3	2	2	3.02	6.19
1	0	0	sa	0.00	4	0	0	5.36	0.99
1	1	1	9.27	4.18	4	1	1	6.68	4.33
2	0	0	34.96	40.35	5	0	0	sa	0.00
2	1	1	12.02	10.19	5	1	1	1.77	0.27
3	0	0	sa	0.00					
			(c) Data Derived from the Crystal Tilted at 41°						
0	4	0	13.34	17.99	2	2	2	(0.72)	1.66
1	0	1	8.89	1.38	2	3	2	1.13	4.42
1	1	1	14.60	4.18	2	4	2	7.38	2.06
1	2	1	(0.72)	1.35	2	5	2	3.11	3.52
1	3	1	6.24	5.31	3	0	3	(0.72)	5.08
1	4	1	9.59	8.83	3	1	3	8.25	7.34
1	5	1	3.36	1.01	3	3	3	1.91	1.24
2	0	2	9.86	1.82	4	0	4	7.72	4.20
2	1	2	9.28	4.73	4	1	4	1.91	5.84

[a] sa designates systematic absence arising rom space group symmetry. Numbers in parentheses designate a threshold "observed" intensity assigned to reflections which are too weak to resolve from the background.

Table III
Summary of Varied Parameters and Their Final Values

parameter	final value
θ[O(5)–C(1)–O(1)–C(4′)]	−81.14°
θ[C(1)–O(1)–C(4′)–C(5′)]	−160.80°
θ[O(6)–C(6)–C(5)–C(4)]	148.95°
μ	56.36°
w	0.6458
atten	3.546

axes parallel to a or b is critical to discriminating between parallel and antiparallel packing models for chiral polymers. In moving from two-dimensional to three-dimensional crystallography, it is necessary to precisely rotate the crystal about a^* or b^*, thereby bringing higher zones into focus. Since a, b, and γ are already known, it is then possible to determine c and β from rotations about a^* and c and α from rotations about b^*. For a correct assessment of symmetry involving the third dimension, it is necessary to rotate the same crystal by $\pm\theta$. It is only, as in the present case, when the identity of the two resulting patterns from each pair of rotations can be established that the orthogonality of c^* to a^* and b^* can be proven and that an orthorhombic space group can be established.

In combination, these techniques provide the most accurate experimentally attainable values of the lattice constants and demonstration of symmetry elements, minimizing the number of space groups which must be considered in modeling. In this present study some space group choices, i.e., these involving parallel chains, were carried past the crystallographic stage. However, in each case the restrictions on symmetry implicit in the crystallography were supported by subsequent structure factor calculations.

In determining molecular structure and packing from the electron diffraction data, it is necessary to distinguish between the base plane contributions arising from untilted crystals and the hkl data derived from tilted crystals. In this study only the simplest possible data reduction was employed; i.e., the intensities were averaged over symmetry-related positions and background scattering was subtracted. No corrections for dynamic scattering or effects arising from bent crystals were applied, although a series of exposures at different times was used to establish the absence of significant sample degradation in the beam. Under these conditions the $hk0$, data derived from untilted crystals lead to conclusions qualitatively similar to those of Nieduszynski.[1] However, the well-defined symmetry and absence of composite reflections permitted a definitive rejection of parallel chain models since such arrangements are inconsistent with the existence of 2_1 axes parallel to either a or b. Arbitration between the remaining antiparallel alternatives was also aided by the absence of composite reflections typical of X-ray fiber diffraction data. Unlike the X-ray study,[1] no expected reflections remained unaccounted for in the $hk0$ data set.

For the data derived from the tilted samples the immediate problem was the question of scaling between these diffraction patterns and the base plane data. Initially, we thought to use the reflections lying on the intersections, e.g., the $h00$ reflections common to $hk0$ and hkk. Since only $h = 2n$ is observed, this leads to two or at most three reflections for scaling. Alternatively, one can ask how well the model derived from the $hk0$ data set coupled to helix symmetry constraints and packing analysis as in eq 1 predicts the intensities of general planes, hkl. We therefore rescaled the data from each higher zone to the $hk0$ derived model. This leads to initial R and R'' values of 0.356 and 0.382, respectively, for 71 reflections. Attempts at continuing the refinement of packing parameter and conformation angle values from this point did not result in any improvement over the values obtained with the $hk0$ data alone, leading us to conclude that there are additional factors that are not being adequately accounted for in our data reduction methodology. These factors might include (a) differences in the interaction of a bent crystal with the electron beam as a function of tilt angle; (b) changes in the linear absorption coefficient with orientation; (c) changes in the sampled surface area of the crystallite with orientation; (d) volume fraction corresponding to each diffracted beam may not be the same; (e) crystal damage effects may be more extensive in the data derived from tilted crystals, since some preliminary irradiation is required to locate and orient the crystal along the tilt axis of the electron microscope prior to the actual data collection. Thus the irradiation dosage is always higher for tilted crystals than for untilted ones, and this may influence the observed intensities.

Despite the small number of layers that can be expected to contribute to scattering from the tilted specimens, there are no detectable subsidiary maxima as might be expected from a small crystallite. The simplest conclusion to be drawn from our work is that the electron diffraction data provide highly reliable lattice constants, tests for symmetry elements, and base plane structure amplitudes while there appears to be additional factors precluding the direct incorporation of higher layer intensity data into the modeling procedure. Further work in which sample degradation effects, crystal bending, and dynamic scattering are considered is now in progress.

The structure derived from the $hk0$ structure amplitudes using all terms in eq 1 is devoid of any overshort inter- or intramolecular contacts. The shortest H···H interaction is 0.214 nm, and all intermolecular C···C interactions are greater than 0.340 nm. These facts coupled with support for a similar model as the preferred choice from X-ray fiber diffraction considerations,[1] a hydrogen-bonding model in which all expected donors and acceptors are involved in attractive interactions, and the tendency of the overall isotropic temperature factor, atten, to remain small but positive when allowed to vary in the final refinement stages all lead us to have a high degree of confidence in the proposed structure. In this context it is interesting to note that the calculations described herein are based predominantly on the intensity data set since its contribution to Ω was 18.7 while the corresponding contribution from the contact calculation was only 0.0958.

The clear choice of an antiparallel packing arrangement in mannan I is in direct opposition to the conclusions drawn for its glucan analogue, native cellulose.[2,3] This choice is also supported by recent ^{13}C CP/MAS NMR data showing precisely six well-resolved resonances for ivory nut mannan with no indication of splittings arising from magnetic anisochrony of chemically equivalent carbon

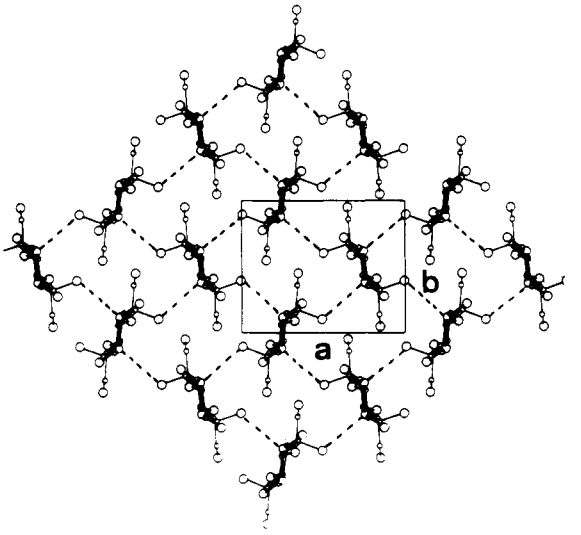

Figure 8. Structure of mannan I viewed as a projection of the unit cell into the ab plane and outlining the shape of the crystals with their (110) growth plane. In this projection each mannan chain is viewed with its helix axis vertical.

Table IV
Summary of Hydrogen Bond Interactions Stabilizing the Structure of Mannan I from Ivory Nut

donor atom	acceptor atom	dist, nm × 10^3	angle, deg	symmetry[a]
O3′	O5	238	101.4 (C3′–O3′···O5)	I···I
O2	O5	311	118.2 (C2–O2···O5)	I···II
O6	O3′	271	115.0 (C6–O6···O3′)	I···I

[a] I···I = intramolecular interactions. I···II = intermolecular interaction, unit II is generated by $(x', y', z') = (-x + a, y + b/2, -z + c/2)$.

atoms.[28] The biosynthetic extrapolation of this result is that synthesis and crystallization of ivory nut mannan are separable events in time and, possibly, location. Mannan chains, having a much lower DP than native cellulose, apparently are dispersed in the cellular milieu where they organize into ordered, ultimately crystalline domains.

Antiparallel packing in which the molecular axis of each mannan chain is coincident with a crystallographic 2_1 axis is stabilized by, at least, two hydrogen bonds per mannosyl residue. Each residue acts as both donor and acceptor in an O2···O5 hydrogen bond as shown in Figure 8A. Additionally, an intramolecular O6···O3′ hydrogen bond is also possible. Distances and the associated $C–O_d···O_a$ angles for these and the intramolecular O3′···O5 hydrogen bond are summarized in Table IV. The O2···O5 and O3′···O5 distances are slightly outside the usual ranges for hydrogen bonds, but this is only a consequence of our reluctance to vary the ring geometry with a limited amount of intensity data. Distortions in ring conformation angles of about 5° and of 2–3° in the exocyclic C–C–O bond angles are sufficient to reduce the O2···O5 distance to 0.28 nm and increase the O3′···O5 distance to more than 0.26 nm. Although this structure can easily be viewed as a three-dimensional hydrogen-bond-stabilized network, one can also envisage sheets of molecules parallel to the 100, 010, or 110 planes. The network description is consistent with the insolubility of native mannan. However, the growth habit evident in Figure 2 implies that for the low molecular weight materials used in this study, crystal growth occurs on the 110 surfaces. This should not be construed as an argument for chain folding since the DP_n of only 13 corresponds to a contour length of less than 7.0 nm, too short for such a morphology. The calculated density of 1.63 $g·cm^{-3}$ agrees reasonably well with the measured value[10]

of 1.57 g·cm^{-3} and indicates the absence of interstitial or site bound water in the structure. The smaller measured value for the density is a consequence of both defects in the crystals and surface free energy effects.

A structural aspect of particular interest is the constancy of two of the lattice edges, *a* and *c*. Comparison of our and other results for mannan I with published data for guar,[6,8] tara,[6,7] and carob[6,8] gums as well as with lattice constants for more highly substituted galactomannans such as fenugreek and lucerne[29] shows that these two dimensions are conserved irrespective of the galactose to mannose ratio. One rationale explanation of this observation is that the sheetlike structure in the *ac* plane is preserved forming a mannan sheet with an irregular coating of galactosyl units on each of its surfaces.[8]

Acknowledgment. W.T.W. gratefully acknowledges partial support of his contribution to this work by the donors of the Petroleum Research Fund, administered by the American Chemical Society, and Centre National de la Recherche Scientifique. D.P.M. was a recipient of a visiting Professorship of the University of Grenoble and G.P. was supported for 1 year by a joint fellowship from the Centre National de la Recherche Scientifique (France) and the Consiglio Nazionale delle Ricerche (Italy).

Registry No. D-Mannan, 9036-88-8.

References and Notes

(1) Nieduszynski, I.; Marchessault, R. H. *Can. J. Chem.* **1972**, *50*, 2130.
(2) Sarko, A.; Muggli, R. *Macromolecules* **1979**, *7*, 486.
(3) Gardner, K. H.; Blackwell, J. *Biopolymers* **1974**, *13*, 1975.
(4) Chanzy, H.; Henrissat, B. *FEBS Lett.* **1985**, *184*, 285.
(5) Frei, E.; Preston, R. D. *Proc. R. Soc. London, B* **1968**, *169*, 127.
(6) Marchessault, R. H.; Buleon, A.; Deslandes, Y.; Goto, T. *J. Colloid Interface Sci.* **1979**, *71*, 375.
(7) Chien, Y. Y.; Winter, W. T. *Macromolecules* **1985**, *18*, 1357.
(8) Bouckris, H.; Winter, W. T., submitted for publication in *Macromolecules*.
(9) Meier, H. *Biochim. Biophys. Acta* **1958**, *28*, 229.
(10) Preston, R. D. *Physical Biology of Plant Cell Walls*; Chapman and Hall: London, 1974; pp 239–255.
(11) Bittiger, H.; Husemann, E. *J. Polym. Sci., Polym. Lett. Ed.* **1972**, *10*, 367.
(12) Chanzy, H.; Dube, M.; Marchessault, R. H.; Revol, J. F. *Biopolymers* **1979**, *18*, 887.
(13) Chanzy, H. D.; Grosrenaud, A.; Joseleau, J. P.; Dube, M.; Marchessault, R. H. *Biopolymers* **1982**, *21*, 301.
(14) Meyer, K. H.; Mark, H. *Der. Aufbau der Hochpolymeren Organischen Naturstoffe*; Akadem. Verlags Gesellschaft: Leipzig, 1930; p 168.
(15) Zugenmaier, P. *Biopolymers* **1982**, *13*, 1127.
(16) Mackie, W.; Sheldrick, B.; Akgrigg, D.; Pérez, S. *Int. J. Biol. Macromol.* **1986**, *8*, 43.
(17) Marchessault, R. H.; Pérez, S. *Biopolymers* **1979**, *18*, 2369.
(18) Timell, T. E. *Can. J. Chem.* **1957**, *35*, 333.
(19) Lüdtke, M. *Ann. Chem. Liebigs* **1927**, *456*, 201.
(20) Chanzy, H.; Excoffier, G.; Guizard, C. *Carbohydr. Polym.* **1981**, *1*, 67.
(21) Miller, D. P.; Brannon, R. D. In *Fiber Diffraction Methods*; French, A. D., Gardner, K. H. C., Eds.; ACS Monograph No. 141; American Chemical Society: Washington, DC, 1980; p 93.
(22) Miller, D.; Chanzy, H.; Paradossi, G. *J. Phys. (Les Ulis, Fr.)* **1986**, *47*, 95.
(23) *International Tables for X-Ray Crystallography*; Kynoch: Birmingham, U.K., 1974; Vol. IV, p 152.
(24) Smith, P. J. C.; Arnott, S. *Acta Crystallogr., Sect. A: Cryst. Phys., Diffr., Theor. Gen. Crystallogr.* **1978**, *A34*, 3.
(25) Arnott, S.; Scott, W. E. *J. Chem. Soc., Perkin Trans. 2* **1972**, 324.
(26) Arnott, S.; Winter, W. T. *Fed. Proc.* **1977**, *36*, 73.
(27) The crystallographic residuals R and R'' are calculated as follows: $R = \sum(k_o F_m - {}_c F_m)2/\sum k^2{}_o F_m{}^2$ and $R'' = \sum[w_m(k^2{}_o F_m{}^2 - {}_c F_m{}^2)]/\sum w_m k^2{}_o F_m{}^2$.
(28) Marchessault, R. H.; Taylor, M. K.; Winter, W. T., submitted for publication in *Macromolecules*.
(29) Song, B. K.; Winter, W. T.; and Taravel, F. R. *Macromolecules*, in press.

Determination of Substituent Distribution in Cellulose Ethers by Means of a ^{13}C NMR Study on Their Acetylated Derivatives. 1. Methylcellulose

Yasuyuki Tezuka* and Kiyokazu Imai*

Department of Material Science and Technology, Technological University of Nagaoka, Kamitomioka, Nagaoka, Niigata 940-21, Japan

Mitsuyoshi Oshima and Tohru Chiba

Shin-Etsu Chemical Co., Ltd., Specialty Chemicals Research Center, 28-1, Nishifukushima, Kubiki, Nakakubiki-gun, Niigata 942, Japan. *Received December 29, 1986*

ABSTRACT: The distribution of methyl groups in methylcellulose having various degrees of substitution was determined by means of ^{13}C NMR analysis after the acetylation of the unsubstituted hydroxyl groups of the parent methylcellulose. The acetyl carbonyl carbon signal of the acetylated methylcellulose samples was found to be split into a triplet in DMSO at 100 °C corresponding to the position of the substituent (2, 3, or 6) on the anhydroglucose unit, allowing the determination of the methyl substituent distribution of methylcellulose samples. The ^{13}C NMR assignment of the split methoxy methyl carbon signal of acetylated methylcellulose samples observed in chloroform solution at 30 °C is proposed with the aid of the substituent distribution analysis by the GLC technique. The methoxy methyl carbon signal was found to be sensitive not only to its substitution position but also to the type of the substituent on the other substitution position.

Introduction

Cellulose derivatives, produced through the reaction of hydroxyl groups in the 2-, 3-, and 6-positions of the anhydroglucose ring unit, have been widely used in a variety of applications as indispensable polymeric materials based on a natural resource. Since the substituent distribution in addition to the total degree of substitution (DS) is expected to influence the properties of the resulting cellulose derivatives, it is of great importance to develop an analytical system to give precise information on the substit-

0024-9297/87/2220-2413$01.50/0